

Characterization of the Young Open Cluster G144.9+0.4 in the Camelopardalis OB1 Association

C. C. Lin (林建爭)

W. P. Chen (陳文屏)

N. Panwar

*Graduate Institute of Astronomy, National Central University, 300 Zhongda Rd., Zhongli
32001, Taiwan; cclin@astro.ncu.edu.tw*

ABSTRACT

Our star-count analysis of the Two Micron All Sky Survey point sources resulted in an identification of the star cluster G144.9+0.4. The cluster was found, but not characterized, by Glushkova et al. We show that the cluster is physically associated with the CamOB1 association at a distance of about 1 kpc and with an age of 1–2 Myr. Pre-main sequence stars are identified, on the basis of photometric and proper motion data. A total of 91 additional OB star candidates was found in subgroups 1A and 1B, a significant increase from the currently known 43 OB stars. The OB members show an age spread that indicates a sustained star formation for at least the last 10–15 Myr. The young cluster G144.9+0.4 represents the latest episode of sequential star formation in this cloud complex.

Subject headings: infrared: stars – open clusters and associations: general – stars: early-type – stars: pre-main sequence – stars: variables: T Tauri, Herbig Ae/Be

1. Introduction

Hundreds of thousands of open clusters (OCs) should currently exist in the Milky Way galaxy based on the number of OCs present in the solar neighborhood (Piskunov et al. 2006). However, the databases of OCs (Dutra & Bica 2001; Dias et al. 2002; Bica et al. 2003; Dutra et al. 2003; Kronberger et al. 2006; Froebrich et al. 2007) contain only a few

thousand entries that are limited to OCs within 1 kpc. This discrepancy is due partly to dust extinction in the Galactic plane, and partly to a lack of comprehensive all-sky searches for distant systems.

Star clusters are groupings of member stars in a six-dimensional phase space in position and motion. Kinematic studies of star clusters require special instrumentation and are often time-consuming. Initial identification of a star cluster via space grouping, i.e., by the “star-count” technique is relatively straightforward and has been exploited efficiently on wide-field or all-sky surveys (Schmeja 2011). The Two Micron All Sky Survey point source catalog (2MASS; Cutri et al. 2003) provides a uniformly calibrated database of the entire sky in the near-infrared (NIR) wavebands, which allows us to recognize OCs even with moderate dust extinction, i.e., partially embedded, young star clusters. Earlier works by Bica et al. (2003), Dutra et al. (2003), and Froebrich et al. (2007) have indeed found hundreds of previously unknown infrared clusters using the 2MASS catalog.

We have developed a star-count technique to recognize star density enhancements and have applied it to the sky within $|b| < 50^\circ$ using the 2MASS data. Hundreds of density peaks were found. We then used the SIMBAD database to match these peaks with known sources within a radius of $5'$, resulting in 501 OCs, 89 globular clusters, 35 galaxies, 55 galaxy clusters, 11 H II regions, and 24 regions contaminated by neighboring bright stars. A total of 5 candidates remain unaccounted for. One such density peak is G144.9+0.4 (designated as G144) located at $\ell \approx 144^\circ.9$ and $b \approx 0^\circ.4$, or R.A. (J2000) = $03^{\text{h}}39^{\text{m}}16^{\text{s}}.7$, decl. (J2000) = $+55^\circ58'24''$, seen toward the Camelopardalis (Cam) OB1 association (Lin et al. 2012). This cluster candidate was recognized by Glushkova et al. (2010), who used a pipeline (Koposov et al. 2008) to search for star clusters with 2MASS data. However, the cluster candidate was not well characterized by their pipeline, apparently because of the nebulous contamination. The full results of our OC finding will be reported elsewhere. Here we present a characterization of this cluster using photometric and proper motion (PM) measurements, and discuss the context of the cluster amid the OB association and cloud complex.

2. Photometric, Kinematic, and Spectroscopic Data

Our data consist of the 2MASS and *WISE* infrared magnitudes, PPMXL PMs, and our own photometric and spectroscopic observations.

2MASS. The NIR magnitudes for point sources have been obtained from 2MASS to the 10σ limiting magnitudes of J ($1.25 \mu\text{m}$) = 15.8, H ($1.65 \mu\text{m}$) = 15.1, and K ($2.17 \mu\text{m}$) = 14.3, respectively. For our star count analysis, we included only stars with a photometric quality

flag better than “CCC”, which effectively gives a signal-to-noise ratio $(S/N) \geq 5$ and a photometric uncertainty of < 0.2 mag in every band to ensure completeness. Subsequently, to characterize clusters we constrained only stars with a photometric quality flag of “AAA”, which corresponds to a $S/N \geq 10$ and a photometric uncertainty of < 0.1 mag in every band for photometric accuracy.

WISE. The *Wide-field Infrared Survey Explorer* mapped the whole sky at 3.4, 4.6, 12, and 22 μm (designated as *W1*, *W2*, *W3*, *W4*) with an angular resolution of $6''.1$, $6''.4$, $6''.5$, and $12''.0$, and a 5σ point-source sensitivity of 0.08, 0.11, 1 and 6 mJy, respectively, corresponding to Vega magnitudes of $W1 = 16.6$, $W2 = 15.6$, $W3 = 11.3$, and $W4 = 8.0$ (*WISE*; Wright et al. 2010). We exploited the identification scheme to search for potential young stellar objects (YSOs) used by Koenig et al. (2012). The *WISE* point sources within the cluster region are extracted from Vizier.¹ Only sources having 2MASS counterparts are included in the analysis.

PPMXL. In addition to photometric data, kinematic information is also employed to secure the membership in a star cluster. The PPMXL Catalog (Röser et al. 2010) contains stars down to about $V \approx 20$ mag and lists the USNO-B1.0 PMs (Monet et al. 2003) and 2MASS *JHK* magnitudes. The stars with PM uncertainties $> 5.0 \text{ mas yr}^{-1}$ have not been used in our analysis.

Tenagra. Narrow-band imaging observations were carried out using the Tenagra II 0.81 meter $f/7$ telescope in Arizona on 2012 March 30. The CCD camera used an SITe chip with 1024×1024 pixels and a pixel size of $\sim 0''.8$, rendering a field of view of $\sim 15 \times 15 \text{ arcmin}^2$ on the sky. The total exposure times were 540 s for the $H\alpha$ and *R* bands, and 300 s for the *I* band. All images were reduced with standard routines, including dark and bias subtraction and flat-field normalization. SExtractor² was used for photometry. The stellar astrometric solution calibrated with the 2MASS coordinates was calculated with the astrometry package from Astrometry.net.³ The Tenagra data reached about $R \sim 18$ mag. Supplementary $H\alpha$ data for fainter stars were taken from the INT/WFC Photometric $H\alpha$ Survey of the Northern Galactic Plane (IPHAS; Drew et al. 2005).

HCT and LOT. Follow-up spectroscopic observations were taken using the HFOSC on the Himalayan Chandra Telescope (HCT) with a slit width of $1''.15$ and Grism 8 ($\lambda = 5800\text{--}8350 \text{ \AA}$, dispersion = $1.45 \text{ \AA pixel}^{-1}$) on 2012 July 26. Additional spectra were taken using

¹<http://vizier.u-strasbg.fr/>

²<http://www.astromatic.net/software/sextractor>

³<http://astrometry.net/>

the Hiyoyu spectrograph on the Lulin One-meter Telescope (LOT) with a slit width of $1''.5$ and grating of 300 mm^{-1} ($\lambda = 3800\text{--}7600 \text{ \AA}$) on the night of 2012 November 15. A one-dimensional spectrum was extracted from the dark, bias-subtracted and flat-field-corrected image in the standard manner using IRAF. The wavelength calibration was done using FeNe (HCT) or HeNeAr (LOT) lamp sources.

3. Characterization of the Cluster

G144 was first recognized by Glushkova et al. (2010), who used the pipeline developed by Koposov et al. (2008) to search for density peaks in a star catalog as star clusters. They found 153 previously unknown clusters within the Galactic latitude $|b| < 24^\circ$, 23 of which were considered to be embedded star clusters and were not characterized by their pipeline. This candidate was also detected as a density peak by our pipeline. In this section, we present the properties of the cluster derived from our analysis.

3.1. Density Enhancements and Radial Density Profile

We selected the 2MASS point sources with $S/N \geq 5$ in J, H, K bands within $15'$ of the apparent center of the cluster. Figure 1 shows the stellar density map for which the number of stars in a grid, whose scale was chosen to include an average of 10 stars, was counted. The resulting density map was then smoothed with a 3×3 grid width. For G144, a background density of $\sim 3.1 \text{ stars arcmin}^{-2}$ was estimated by 3σ clipping of the density outliers. A grid in the smoothed density map 3σ above the background would be considered a high-density region, and a grouping of more than three connected high-density regions would be identified as a density enhancement, i.e., a cluster candidate. The density map around G144 is shown in Figure 1.

We estimated the size of G144 based on the radial density profile, though the cluster appears slightly elongated in shape. As seen in Figure 2, the density starts to blend with the field at a radius of $\sim 3'.5$. We therefore adopted a radius of $3'.5$ for the cluster in subsequent analysis. Spatially the cluster is seen near the Cam OB1 association and is likely physically related to it.

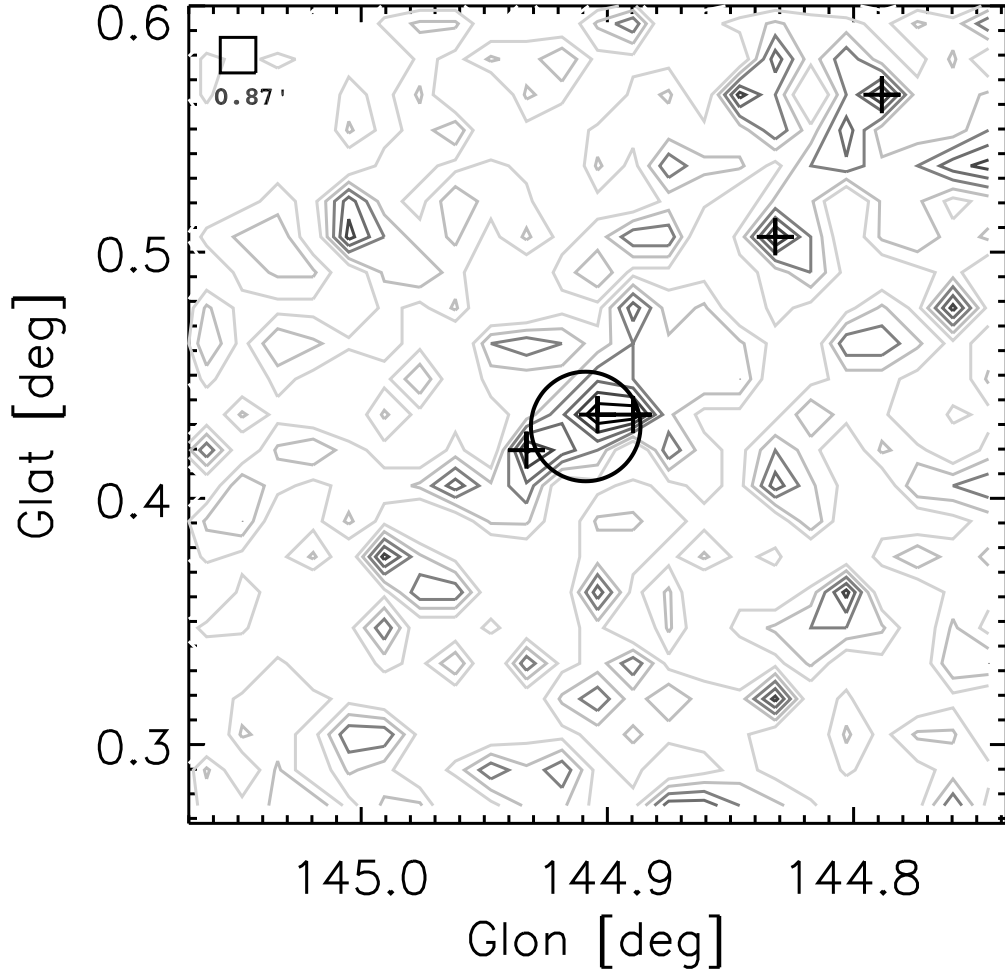


Fig. 1.— Stellar density map of G144. The pluses mark the grids 3σ above the average density. The circle shows the effective size, which is estimated from the three neighboring pluses.

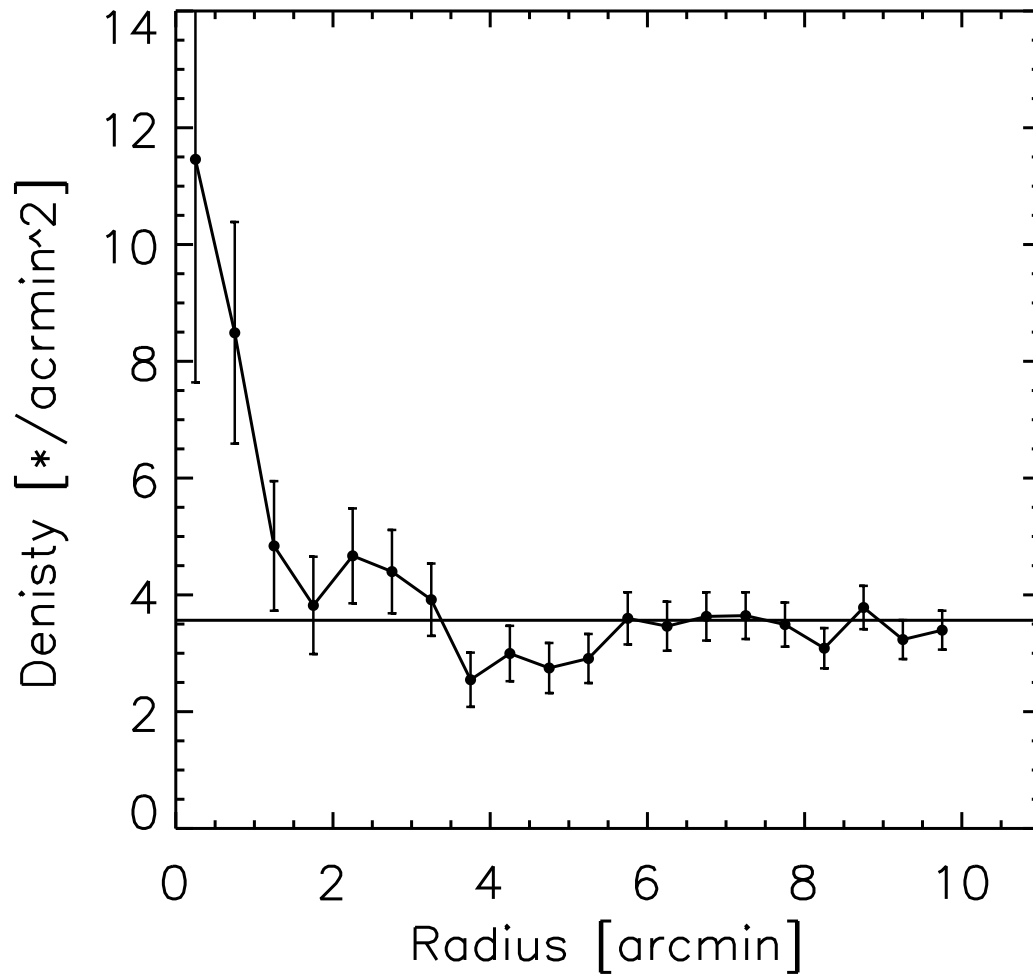


Fig. 2.— Radial density profile for G144. Filled dots are surface stellar density values with each error bar estimated by Poisson statistics. The horizontal line depicts the background density. The oscillation between the radius of 2' and 4' is due to the elongated shape of the cluster.

3.2. Proper Motion Members

Cluster members share the same age, metallicity, distance, PMs, etc. Accordingly, common PMs would be a necessary condition for cluster membership. The Cam OB1 association was first investigated by Morgan et al. (1953), who found eight early-type stars aggregated at a distance of ~ 900 pc. Several studies, e.g., Haug (1970), Humphreys (1978), and Lyder (2001), append the members of Cam OB1. However, the Cam OB1 members spread over an area on the sky of $\sim 20 \times 10$ deg² corresponding to a physical dimension of $\sim 320 \times 160$ pc², making a coeval formation of the Cam OB1 impossible (de Zeeuw et al. 1999). Straizys & Laugalys (2007a) divided the association into three subgroups—1A, 1B, and 1C—and found them all at nearly the same distance of ~ 1 kpc. G144 is located between 1A and 1B, which contain 30 and 13 OB stars, respectively (Straizys & Laugalys 2007a). The other subgroup, 1C, has 76 known members mainly from NGC 1502 (Weitenbeck 1997).

To provide the criteria for selecting PM members in G144, we first extracted the PPMXL PMs of the known OB stars. The same data would also allow us to identify faint OB members that might have escaped recognition in previous works. The derived PPMXL PMs of each subgroup are $(\mu_\alpha, \mu_\delta) = (-1.1 \pm 2.1, -1.9 \pm 1.5)$ mas yr⁻¹ for 1A, $(\mu_\alpha, \mu_\delta) = (-0.8 \pm 0.6, -2.3 \pm 1.0)$ mas yr⁻¹ for 1B, and $(\mu_\alpha, \mu_\delta) = (-0.2 \pm 1.5, -0.4 \pm 2.5)$ mas yr⁻¹ for 1C. Indeed the three subgroups share similar PMs, suggesting a physical association. The parameters for the three subgroups, including the PMs, are summarized in Table 1.

To identify previously unknown OB stars, we select stars within the same area $\sim 10 \times 10$ deg², as that of the known Cam OB1 association centered on Cam OB1A and 1B, respectively, which are (1) photometrically consistent with OB spectral types in the NIR color–magnitude diagram (CMD), and (2) kinematically consistent with the systemic PM of the 1A and 1B subgroups. The CMD criteria are 2MASS J brighter than 13.0 mag and $J - H < 0.2$ mag. Only stars with photometric uncertainties better than 0.02 mag in every 2MASS band were considered. The PM criteria include uncertainties less than 5 mas yr⁻¹ and within the 3σ range of the mean PM of 1A and 1B, as shown in Figure 3. Table 2 lists the 68 and 23 newly found OB stars in 1A and 1B, respectively. The first column gives the numerical identification of the stars, in order of descending brightness, followed by subsequent columns listing the Galactic coordinates, 2MASS magnitudes, and PPMXL PMs of each star. The last column lists the data belonging in 1A or 1B. The photometric and color properties of these newly found OB stars will be discussed later together with the cluster members.

For cluster members, there are 23 stars that are spatially within the 3.5 radius and kinematically within the 3σ range of the average PM of the known OB stars, as shown in Figure 4 and listed in Table 3. Again, only stars with PPMXL uncertainties less than

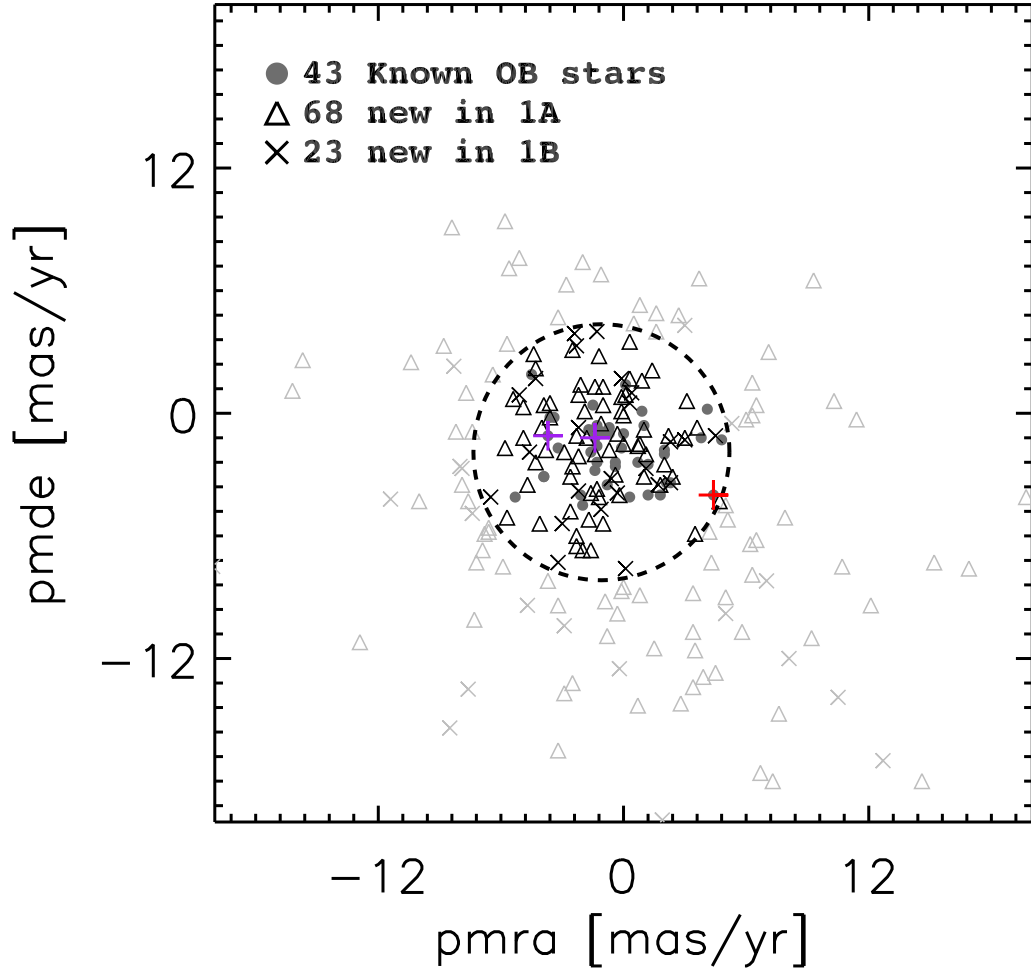


Fig. 3.— Newly identified OB stars in Cam OB1A and 1B. The filled circles mark known Cam OB1 members (Straizys & Laugalys 2007a), and the two purple and one red pluses are supergiants with $J - H$ larger than 0.5 mag (discussed in Session 3.4). The dashed circle is the 3σ range of the mean PMs of known OB stars in Cam OB1A and 1B. Triangles are OB star candidates in 1A and crosses are those in 1B. Symbols in black represent those with PMs consistent with being members.

5 mas yr^{-1} were selected. The PM candidates need to be further winnowed by photometric selection as discussed in the next section.

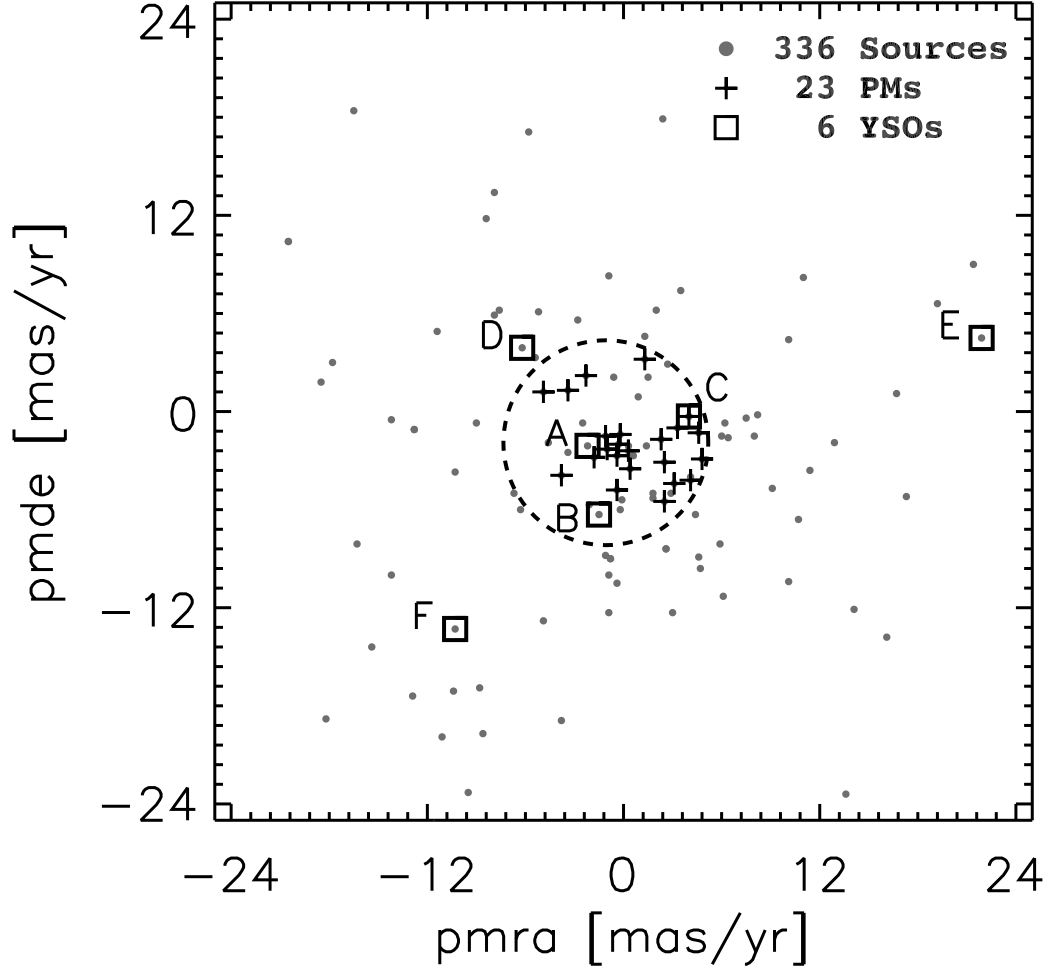


Fig. 4.— Stellar proper motions toward G144. Stars within a $3'.5$ radius of the cluster are represented by gray dots. The dashed circle, as in Figure 3, shows the probable PM range for membership. Pluses mark PM candidates. Boxes, individually labeled, are stars with infrared excess or highly reddened colors (discussed in Session 3.3).

Table 1. Three Subgroups of the Cam OB1 Association

Subgroup	ℓ, b (deg)	Angular Size (deg)	Distance (pc)	Age (Myr)	No. of Stars	μ_{α}^{d} (mas yr ⁻¹)	μ_{δ}^{d} (mas yr ⁻¹)
1A	140.0, +1.5	$\sim 10 \times 10$	1010 ± 210	$\lesssim 10^{\text{a}}$	30 ^a	-1.1 ± 2.1	-1.9 ± 1.5
1B	148.0, -0.5	$\sim 10 \times 10$	~ 1000	$\lesssim 10^{\text{a}}$	13 ^a	-0.8 ± 0.6	-2.3 ± 1.0
1C	143.7, +7.7	0.1	1180 ± 160	$\sim 10^{\text{c}}$	76 ^b	-0.2 ± 1.5	0.4 ± 2.5

^aStraižys & Laugalys (2007a).

^bMostly NGC 1502 members (Weitenbeck 1997).

^cPaunzen et al. (2005).

^dDerived from PPMXL.

Table 2. New OB Candidates in Cam OB 1A and 1B

ID	ℓ, b (deg)	J (mag)	H (mag)	K (mag)	μ_α (mas yr ⁻¹)	μ_δ (mas yr ⁻¹)	Comments
1	136.423, -0.948	6.68	6.53	6.44	-0.1 ± 0.9	0.1 ± 0.7	1A
2	135.499, +0.833	7.31	7.14	7.02	-3.6 ± 1.1	-0.2 ± 0.8	1A
3	139.336, +2.513	8.31	8.31	8.26	-5.8 ± 1.0	-1.7 ± 0.9	1A
4	135.552, +2.559	8.73	8.65	8.57	-1.0 ± 1.8	-5.4 ± 1.8	1A
5	135.575, +1.579	8.89	8.82	8.76	-0.1 ± 1.4	0.8 ± 1.1	1A
6	139.909, +0.635	9.16	9.05	8.95	0.3 ± 1.8	1.7 ± 1.7	1A
7	142.940, -0.745	9.23	9.19	9.12	-1.3 ± 1.3	-3.7 ± 1.3	1A
8	139.404, +2.266	9.26	9.17	9.12	0.8 ± 1.6	-1.5 ± 1.6	1A
9	143.240, -1.364	9.29	9.19	9.10	-4.9 ± 1.8	0.3 ± 1.8	1A
10	144.540, +4.802	9.30	9.29	9.25	-4.3 ± 1.1	2.2 ± 1.0	1A
11	140.150, +2.163	9.39	9.37	9.32	-2.2 ± 1.6	0.9 ± 1.7	1A
12	142.818, +2.377	9.55	9.44	9.37	-1.1 ± 2.1	-0.5 ± 2.1	1A
13	135.773, +1.449	9.73	9.65	9.60	-3.9 ± 2.0	0.4 ± 2.0	1A
14	141.764, -2.567	9.79	9.63	9.53	-4.9 ± 2.9	-1.2 ± 2.9	1A
15	139.879, +4.601	9.83	9.75	9.69	-1.4 ± 1.9	1.3 ± 1.9	1A
16	144.565, +1.886	9.95	9.80	9.71	-4.4 ± 1.6	2.9 ± 1.6	1A
17	140.789, +2.781	9.95	9.78	9.68	0.3 ± 2.0	3.5 ± 2.0	1A
18	143.333, -0.103	9.96	9.82	9.76	-0.2 ± 2.1	-4.0 ± 2.1	1A
19	144.446, -1.431	10.04	9.86	9.76	-2.9 ± 2.1	-1.9 ± 2.1	1A
20	143.361, +3.974	10.06	9.95	9.87	-0.3 ± 1.7	-1.0 ± 1.7	1A
21	143.964, +3.254	10.25	10.17	10.12	1.1 ± 2.1	-2.0 ± 2.1	1A
22	144.320, +5.428	10.27	10.28	10.28	-4.3 ± 1.6	-2.4 ± 1.6	1A
23	137.583, +4.872	10.35	10.15	10.10	1.8 ± 2.0	-3.5 ± 2.0	1A
24	143.845, +5.805	10.37	10.22	10.17	-1.2 ± 1.9	2.8 ± 1.9	1A
25	136.891, +5.032	10.40	10.20	10.15	-1.0 ± 1.7	1.3 ± 1.7	1A
26	139.130, +1.675	10.41	10.22	10.14	-2.5 ± 1.7	-2.6 ± 1.7	1A
27	141.658, +1.215	10.46	10.35	10.27	-5.7 ± 2.3	-5.1 ± 2.3	1A
28	143.742, +1.059	10.46	10.32	10.24	-1.0 ± 2.2	0.4 ± 2.2	1A
29	143.141, +3.525	10.46	10.38	10.29	-1.9 ± 1.8	0.1 ± 1.8	1A
30	138.041, -0.551	10.49	10.40	10.31	-1.8 ± 2.1	-1.2 ± 2.1	1A
31	143.335, -0.101	10.50	10.37	10.27	-0.4 ± 2.2	-3.0 ± 2.2	1A
32	144.343, +4.769	10.51	10.35	10.28	-2.5 ± 1.7	3.1 ± 1.7	1A
33	143.773, +2.906	10.56	10.42	10.31	0.0 ± 1.8	-1.5 ± 1.8	1A
34	143.795, +3.308	10.56	10.42	10.35	0.7 ± 1.8	-1.6 ± 1.8	1A
35	139.743, +4.774	10.59	10.44	10.29	3.6 ± 2.7	-0.7 ± 2.7	1A
36	140.181, +2.158	10.63	10.52	10.48	-4.1 ± 2.0	-5.4 ± 2.0	1A
37	141.804, +2.273	10.66	10.55	10.48	3.5 ± 1.8	-5.9 ± 1.8	1A
38	144.248, +2.220	10.67	10.54	10.47	0.9 ± 1.8	1.6 ± 1.8	1A
39	142.569, +0.978	10.70	10.53	10.43	-1.4 ± 1.9	-2.0 ± 1.9	1A
40	143.314, -0.222	10.76	10.66	10.60	2.0 ± 1.6	-2.5 ± 1.6	1A
41	138.486, +3.456	10.77	10.59	10.54	2.4 ± 2.7	-3.1 ± 2.7	1A
42	135.654, +1.584	10.78	10.77	10.71	1.0 ± 2.0	-0.8 ± 2.0	1A
43	144.849, -2.906	10.82	10.67	10.48	-2.2 ± 4.1	-2.1 ± 4.1	1A
44	138.594, +2.357	10.85	10.66	10.53	2.2 ± 2.8	-1.1 ± 2.8	1A
45	144.165, +3.279	10.86	10.74	10.67	-2.1 ± 2.1	1.4 ± 2.1	1A

Table 2—Continued

ID	ℓ, b (deg)	J (mag)	H (mag)	K (mag)	μ_α (mas yr ⁻¹)	μ_δ (mas yr ⁻¹)	Comments
46	137.987, -0.541	10.88	10.69	10.58	-1.2 ± 1.8	-4.1 ± 1.8	1A
47	141.849, +2.190	10.95	10.80	10.73	3.0 ± 2.2	-1.2 ± 2.2	1A
48	143.304, -0.146	10.98	10.90	10.78	-2.6 ± 1.8	-4.8 ± 1.8	1A
49	138.642, +2.290	10.99	10.89	10.82	-3.6 ± 2.0	0.5 ± 2.0	1A
50	144.131, -2.173	11.01	10.89	10.82	0.1 ± 1.8	0.9 ± 1.8	1A
51	143.997, +3.374	11.02	10.84	10.74	-1.6 ± 2.1	-3.9 ± 2.1	1A
52	141.297, +2.745	11.04	10.91	10.83	-2.6 ± 2.1	-3.1 ± 2.1	1A
53	143.963, -1.950	11.07	10.93	10.87	-4.7 ± 2.3	-3.5 ± 2.3	1A
54	144.713, +2.623	11.09	10.90	10.80	-2.3 ± 2.2	-1.1 ± 2.2	1A
55	144.094, +2.151	11.10	11.01	10.91	-5.4 ± 1.8	0.7 ± 1.9	1A
56	143.235, +4.009	11.16	11.04	10.95	-2.3 ± 1.7	-6.0 ± 1.7	1A
57	143.371, -0.256	11.19	11.07	11.02	4.7 ± 1.7	-4.3 ± 1.7	1A
58	143.492, -1.700	11.22	11.06	10.96	-2.3 ± 2.3	-6.5 ± 2.3	1A
59	141.780, -2.387	11.24	11.04	10.95	0.0 ± 2.9	-0.1 ± 2.9	1A
60	137.154, +5.389	11.35	11.16	11.09	-1.6 ± 4.1	-6.7 ± 4.1	1A
61	137.392, +3.852	11.38	11.24	11.16	1.0 ± 1.7	-3.1 ± 1.6	1A
62	144.385, +2.014	11.42	11.24	11.13	3.1 ± 2.9	0.6 ± 2.9	1A
63	143.751, +3.354	11.45	11.26	11.19	-4.0 ± 1.8	-0.7 ± 1.8	1A
64	143.183, -1.119	11.49	11.32	11.21	1.4 ± 2.2	2.1 ± 2.2	1A
65	142.926, -0.749	11.53	11.43	11.33	-2.0 ± 2.2	-6.7 ± 2.2	1A
66	144.419, +3.040	11.53	11.39	11.34	-3.8 ± 1.7	-1.8 ± 1.7	1A
67	138.831, +6.303	11.59	11.46	11.37	-0.7 ± 4.0	-1.8 ± 4.0	1A
68	135.975, +1.828	11.88	11.73	11.63	-1.7 ± 2.7	-5.2 ± 2.7	1A
1	146.869, -5.801	6.04	5.89	5.83	0.4 ± 0.6	1.0 ± 0.7	1B
2	145.762, +3.327	9.32	9.20	9.10	-0.6 ± 1.8	-3.2 ± 1.8	1B
3	146.307, -5.275	9.50	9.43	9.36	-0.1 ± 1.4	1.7 ± 1.4	1B
4	146.855, -0.543	9.54	9.39	9.31	-4.6 ± 2.0	-1.9 ± 2.0	1B
5	146.016, +3.242	9.91	9.85	9.81	-2.4 ± 2.1	3.9 ± 2.1	1B
6	146.804, -0.548	9.94	9.83	9.73	-4.3 ± 2.7	1.7 ± 2.7	1B
7	145.503, -6.755	10.21	10.15	10.07	0.3 ± 1.7	0.5 ± 1.7	1B
8	146.309, -0.178	10.40	10.29	10.19	-1.3 ± 1.7	4.0 ± 1.7	1B
9	151.415, +3.612	10.42	10.31	10.22	-2.2 ± 2.0	-0.7 ± 2.0	1B
10	150.306, -6.250	10.44	10.37	10.28	0.1 ± 1.4	-7.6 ± 1.4	1B
11	151.443, +3.504	10.84	10.64	10.56	-6.5 ± 4.0	-4.1 ± 4.0	1B
12	146.497, +3.146	10.86	10.68	10.60	2.3 ± 1.8	-1.4 ± 1.8	1B
13	148.254, +2.582	10.87	10.75	10.70	-2.3 ± 1.8	3.3 ± 1.8	1B
14	148.387, +0.963	11.07	10.93	10.85	4.5 ± 1.7	-1.1 ± 1.7	1B
15	146.421, -5.025	11.14	10.97	10.84	-2.2 ± 4.1	-3.8 ± 4.1	1B
16	146.069, +3.633	11.52	11.47	11.39	-0.3 ± 1.8	-3.9 ± 1.8	1B
17	148.234, +2.526	11.52	11.39	11.30	-5.1 ± 2.2	0.9 ± 2.2	1B
18	146.432, -5.113	11.59	11.39	11.27	-3.0 ± 4.1	-5.4 ± 4.1	1B
19	151.412, +3.551	11.59	11.43	11.34	1.1 ± 4.0	-2.7 ± 4.0	1B
20	145.901, -4.777	11.72	11.58	11.49	-3.2 ± 4.1	-7.3 ± 4.1	1B
21	145.648, -4.026	11.86	11.67	11.56	3.0 ± 4.1	-1.3 ± 4.1	1B
22	156.362, -6.956	11.99	11.89	11.82	-1.1 ± 3.9	-4.7 ± 3.9	1B

3.3. Young Stellar Objects

Straizys & Laugalys (2007b) have used infrared photometric data extracted from 2MASS, *IRAS* and *MSX* to identify 35 YSOs in a region $12 \times 12 \text{ deg}^2$ toward the Cam OB1 association, none of which are located within G144. Nonetheless, nebulosity is clearly seen around G144, suggesting a young age. Generally, YSOs are identified by their infrared excess, $H\alpha$ emission, or X-ray emission. No X-ray data are available in the region, so we used 2MASS and *WISE* to identify possible YSOs or embedded stars in G144.

The NIR-excess sources were identified using the 2MASS ($J - H$) versus ($H - K$) and *WISE* [3.4] – [4.6] versus [4.6] – [12] color-color diagrams, shown in Figure 5 and Figure 6. Three classical T Tauri (CTTS; class II objects) candidates were found in the empirical CTTS region (Meyer et al. 1997) in the 2MASS color-color diagram. On the other hand, using the criteria adopted by Koenig et al. (2012), five CTTS candidates were identified on the basis of the *WISE* colors, two of which coincide with the 2MASS sources. Therefore, a total of six CTTS candidates are selected, whose coordinates, 2MASS and *WISE* magnitudes, and PPMXL PMs are listed in Table 4. The first column gives the alphabetical identification of the star, in order of descending brightness, followed by subsequent columns of Galactic coordinates, 2MASS as well as *WISE* magnitudes, and PPMXL PM of each star. The last column lists the data used for the classification.

The IPHAS r and narrow-band $H\alpha$ magnitudes are used to single out stars with possible $H\alpha$ emission. Figure 7 shows the $r-H\alpha$ versus r -band magnitude. Star A, the brightest among our CTTS candidates, is some $\sim 0.5 \text{ mag}$ brighter in $H\alpha$ than a “normal” star, defined as a star following the trend between the $H\alpha$ - and r -band magnitudes for the majority of stars in the field. Subsequent HCT spectroscopic observations confirmed an emission spectrum for star A, as seen in Figure 8. On the basis of the NIR excess and the emission-line spectrum, we conclude that star A, located near the center of G144, should be a CTTS.

For other YSO candidates, star B, located near the nebulosity edge, has the most reddened NIR colors among our candidates, and is a CTTS candidate judging by both 2MASS and *WISE* colors. It may have weak $H\alpha$ emission (see Figure 7), but, unfortunately, was too faint for our spectroscopic observations. Star B is likely a CTTS. Both stars C and D

Table 2—Continued

ID	ℓ, b (deg)	J (mag)	H (mag)	K (mag)	μ_α (mas yr $^{-1}$)	μ_δ (mas yr $^{-1}$)	Comments
23	145.908, -4.784	12.05	11.87	11.80	1.7 ± 4.1	-3.5 ± 4.1	1B

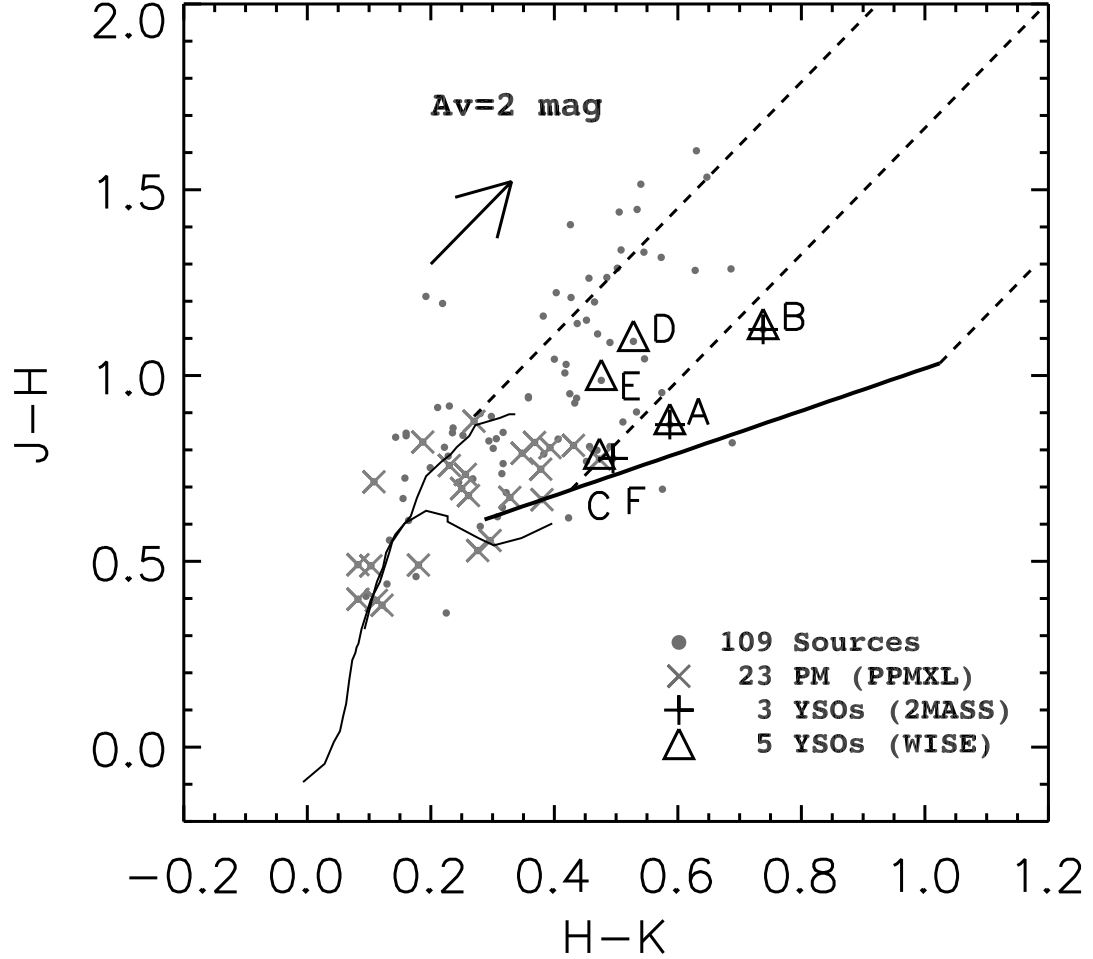


Fig. 5.— 2MASS color-color diagram in the cluster region. Pluses and triangles are CTTS candidates (pluses denote 2MASS sources and triangles denote *WISE*). Crosses represent proper motion members. Gray dots are none of the above. The thin curves show the giant and dwarf loci (Bessell & Brett 1988) converted to the 2MASS system. The thick line is the intrinsic CTTS locus (Meyer et al. 1997). The arrow represents the reddening direction (Rieke & Lebofsky 1985) for typical Galactic interstellar extinction ($R_V = 3.1$), and the dashed lines encompass the region of reddened giants and dwarfs. Stars to the right of this region have NIR excess and are possible YSOs.

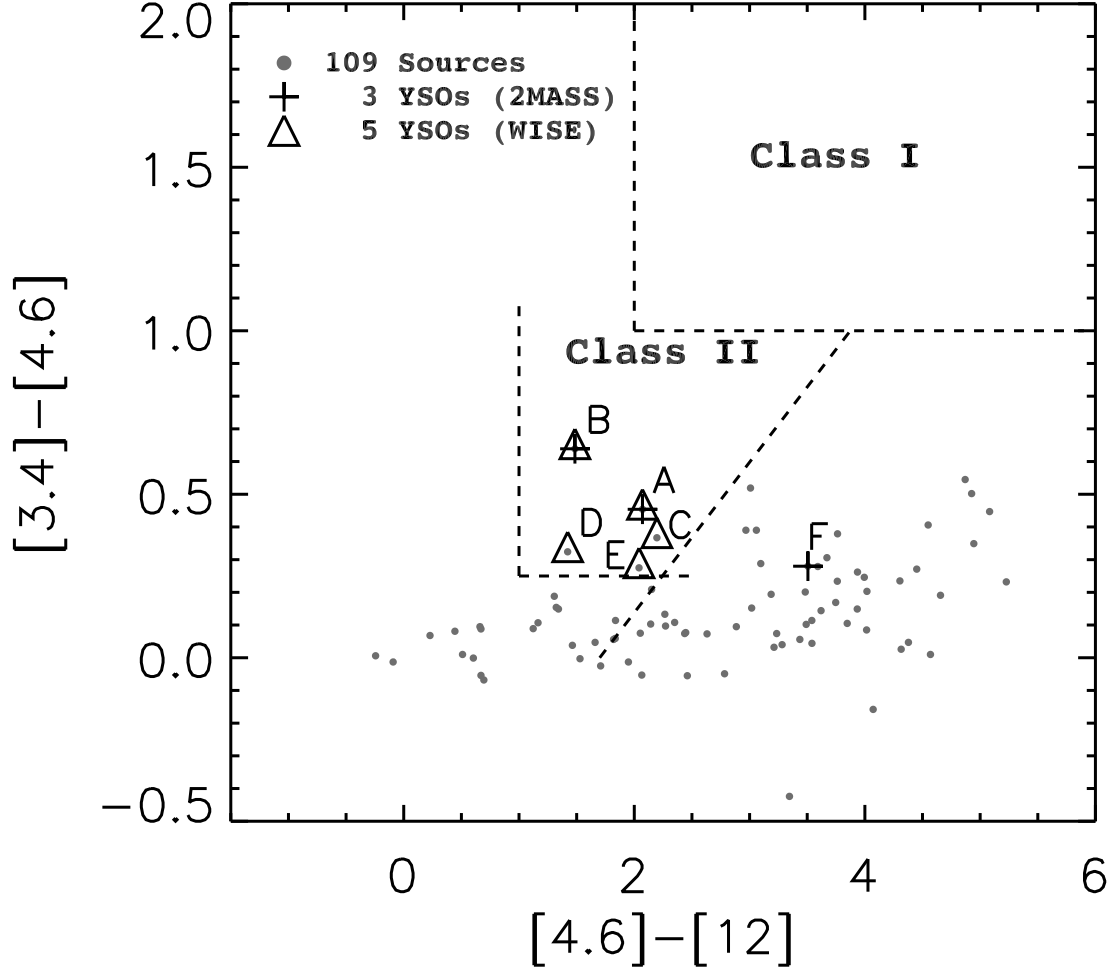


Fig. 6.— *WISE* $[3.4] - [4.6]$ μm vs. $[4.6] - [12]$ μm colors in the cluster region. The dashed lines defined by Koenig et al. (2012) are used to identify Class I and Class II young stellar objects. As in Figure 5, the 2MASS detections are in pluses and the *WISE* detections are in triangles.

Table 3. Proper Motion Member Candidates

ID	ℓ, b (deg)	J (mag)	H (mag)	K (mag)	μ_α (mas yr ⁻¹)	μ_δ (mas yr ⁻¹)
1	144.911, +0.395	11.89	11.50	11.41	-0.4 ± 4.0	-4.8 ± 4.0
2	144.898, +0.437	11.93	11.25	10.99	-4.9 ± 4.0	1.2 ± 4.0
3	144.946, +0.409	12.28	11.53	11.15	-1.0 ± 4.0	-2.3 ± 4.0
4	144.913, +0.418	12.71	12.04	11.71	-0.3 ± 4.0	-2.0 ± 4.0
5	144.903, +0.437	12.96	12.15	11.76	1.3 ± 4.0	3.2 ± 4.0
6	144.891, +0.391	13.12	12.74	12.62	0.3 ± 4.0	-2.4 ± 4.0
7	144.918, +0.420	13.14	12.35	12.00	4.1 ± 4.0	-4.2 ± 4.0
8	144.909, +0.462	13.40	12.91	12.81	2.5 ± 4.0	-5.5 ± 4.0
9	144.940, +0.402	13.43	12.94	12.86	-3.4 ± 4.0	1.3 ± 4.0
10	144.858, +0.449	13.66	13.26	13.15	-0.2 ± 4.0	-1.4 ± 4.0
11	144.917, +0.465	13.69	13.20	13.02	3.1 ± 4.0	-4.4 ± 4.0
12	144.896, +0.430	13.94	13.16	12.69	4.0 ± 4.0	-0.3 ± 4.0
13	144.913, +0.468	14.58	13.91	13.53	-1.8 ± 4.0	-2.8 ± 4.0
14	144.955, +0.436	14.63	13.87	13.64	-3.8 ± 4.0	-3.9 ± 4.0
15	144.928, +0.430	14.67	13.97	13.72	-1.1 ± 4.0	-1.5 ± 4.0
16	144.942, +0.452	14.73	13.92	13.49	3.3 ± 4.0	-1.0 ± 4.0
17	144.862, +0.464	14.85	14.29	14.00	4.8 ± 4.0	-2.9 ± 4.0
18	144.877, +0.401	14.90	14.19	14.08	-0.4 ± 4.0	-2.7 ± 4.0
19	144.906, +0.455	14.92	14.10	13.91	2.5 ± 4.0	-3.1 ± 4.0
20	144.872, +0.473	14.92	14.39	14.11	4.6 ± 4.0	-1.3 ± 4.0
21	144.948, +0.453	15.13	14.31	13.94	0.4 ± 4.0	-3.5 ± 4.0
22	144.915, +0.456	15.43	14.69	14.44	2.3 ± 4.1	-1.7 ± 4.1
23	144.866, +0.404	15.91	15.04	14.77	-2.3 ± 4.1	2.2 ± 4.1

Table 4. YSO Candidates in G144

ID	ℓ, b (deg)	J (mag)	H (mag)	K (mag)	$W1$ (mag)	$W2$ (mag)	$W3$ (mag)	$W4$ (mag)	μ_α (mas yr ⁻¹)	μ_δ (mas yr ⁻¹)	Comments
A	144.895, +0.439	11.4	10.6	10.0	9.4	9.0	6.9	2.9	-2.2 ± 5.0	-2.1 ± 5.0	<i>WISE</i> ; 2MASS
B	144.881, +0.403	13.4	12.3	11.6	10.5	9.8	8.3	6.6	-1.5 ± 5.3	-6.3 ± 5.3	<i>WISE</i> ; 2MASS
C	144.896, +0.430	13.9	13.2	12.7	12.1	11.7	9.5	5.3	4.0 ± 4.0	-0.3 ± 4.0	<i>WISE</i>
D	144.899, +0.426	14.2	13.1	12.6	11.9	11.6	10.2	6.1	-6.2 ± 5.4	3.9 ± 5.4	<i>WISE</i>
E	144.914, +0.412	16.1	15.1	14.6	14.5	14.2	12.1	8.7	21.9 ± 5.5	4.5 ± 5.5	<i>WISE</i> ; non-member
F	144.853, +0.454	16.2	15.4	14.9	14.8	14.5	11.0	8.6	-10.3 ± 5.5	-13.3 ± 5.5	2MASS; non-member

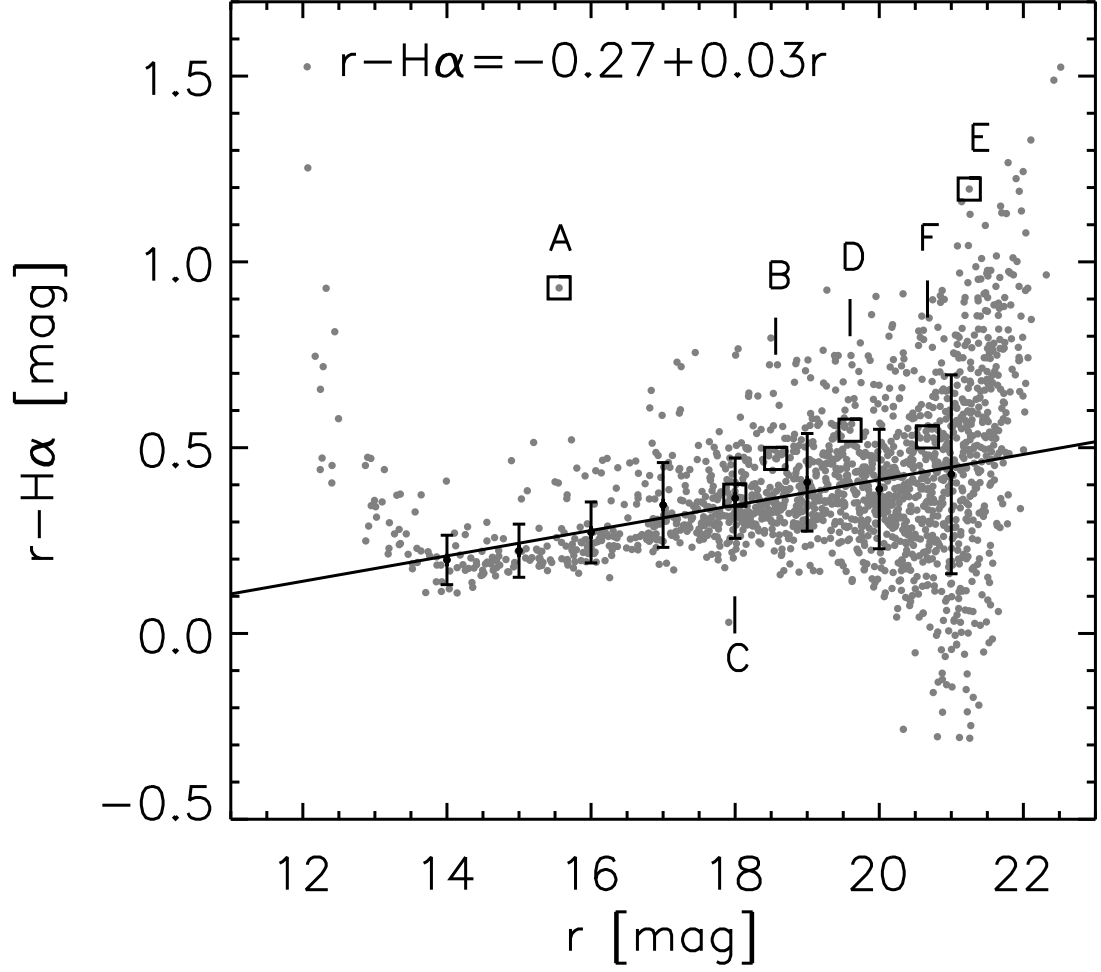


Fig. 7.— IPHAS magnitudes of $r-H\alpha$ vs r . Each YSO candidate is labeled and marked with a box. Bright stars ($r < 14$ mag) are saturated. The typical error, marked for each magnitude, has been estimated by Poisson statistics. The line shows the linear regression of $r-H\alpha$ and r magnitudes of stars between $r \sim 14$ –21 mag.

are both marginal candidates in terms of their PMs and *WISE* colors. Their 2MASS colors do not stand out, though star D, with possible $H\alpha$ in emission, is much more reddened than star C. Both stars E and F are very faint, so have large uncertainties in their PM measurements. They are marginal cases in either 2MASS or *WISE* colors, and seem to have motions inconsistent with membership. Hence, stars E and F should be classified as field stars.

3.4. Extinction, Distance, and Age

The average interstellar extinction to the cluster was estimated by tracing each of the 23 PM candidates back to the MS locus along the reddening vector in the 2MASS color-color diagram (see Figure 5). An average extinction of $A_J \sim 0.56$ mag was derived. Figure 9 plots the J versus $J - H$ CMD for the Cam OB1 subgroups 1A and 1B, as well as for G144. In each case, a zero-age main-sequence (ZAMS) is shown with solar metallicity⁴ at a distance of ~ 1 kpc with corresponding extinction and reddening.

The 1C subgroup has a well constrained age (~ 10 Myr) and distance (~ 1 kpc) because of the cluster NGC 1502 (Tapia et al. 1991; Paunzen et al. 2005). A possible abnormal interstellar reddening has been suggested, as diagnosed by the total-to-selective extinction, $R_V = A_V/E(B - V)$ from 2.42 (Tapia et al. 1991) to 2.57 (Pandey et al. 2003), as compared to the average $R_V = 3.1$ in the diffuse interstellar medium. A reduced value of R_V is indicative of a smaller than typical average grain size, likely as the consequence of photoevaporation by OB stars in the region. The variation of R_V has little effect on our analysis of the properties of G144.

The cluster G144 therefore is at the same distance as the Cam OB1 association which makes it physically a part of that association. The newly found OB stars in 1A (Figure 9, left panel) and 1B (Figure 9, right panel) considerably augment the OB star inventory in the region. For G144 (Figure 9, middle panel), most PM candidates are distributed along the ZAMS. YSO candidates such as stars A, B, and D are located above the MS, i.e., at ages of $\lesssim 1$ Myr and have NIR excess. The existence of CTTSs sets a stringent age limit for the cluster—no more than a couple of megayears.

Figure 10 illustrates the positional distribution of the young stellar population in Cam OB1. Subgroup 1B is associated with a molecular cloud ring (Straižys & Laugalys 2008). It is conceivably a remnant bubble created by a supernova, devoid of gas and dust, and the newly

⁴Available from the Padova isochrone database <http://stev.oapd.inaf.it/cgi-bin/cmd>.

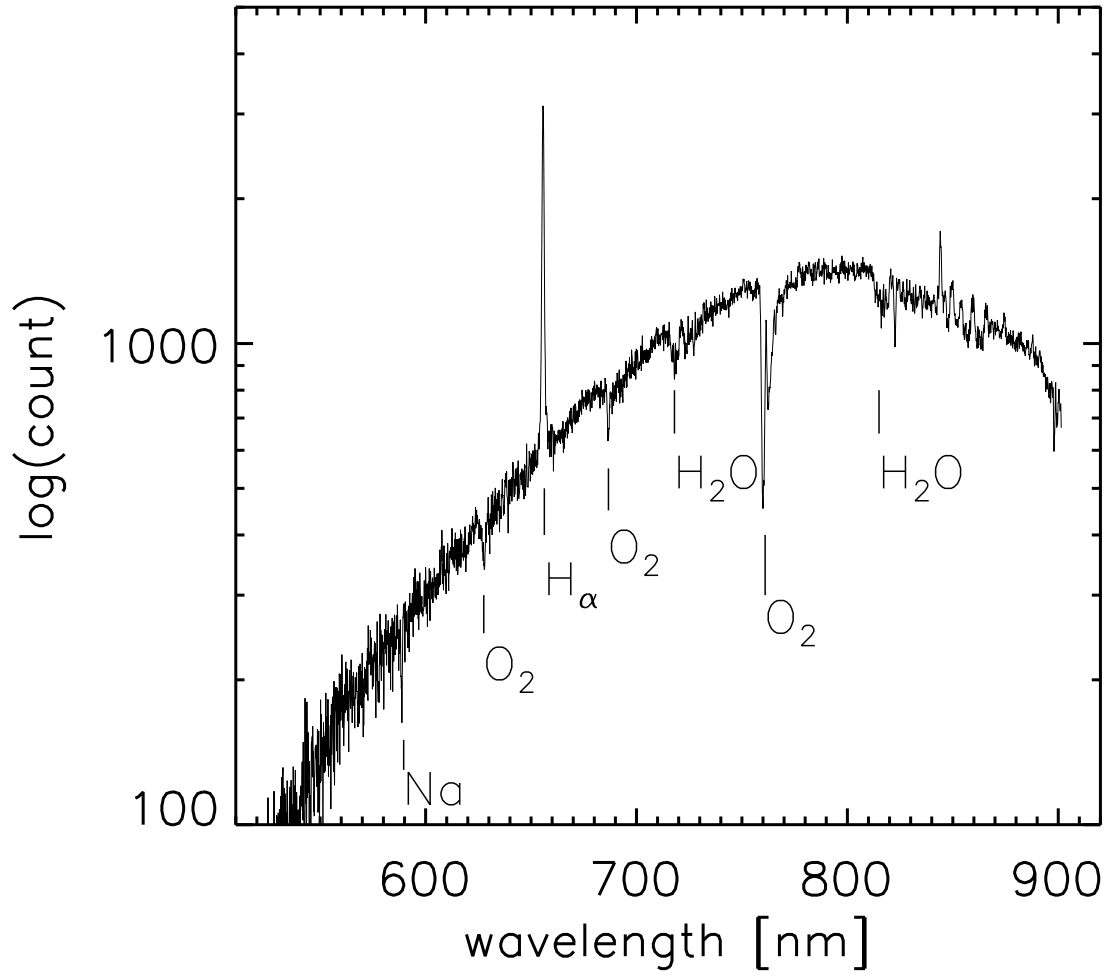


Fig. 8.— HCT spectrum of star A. A prominent $\text{H}\alpha$ emission line is evident. Other spectral features are also marked.

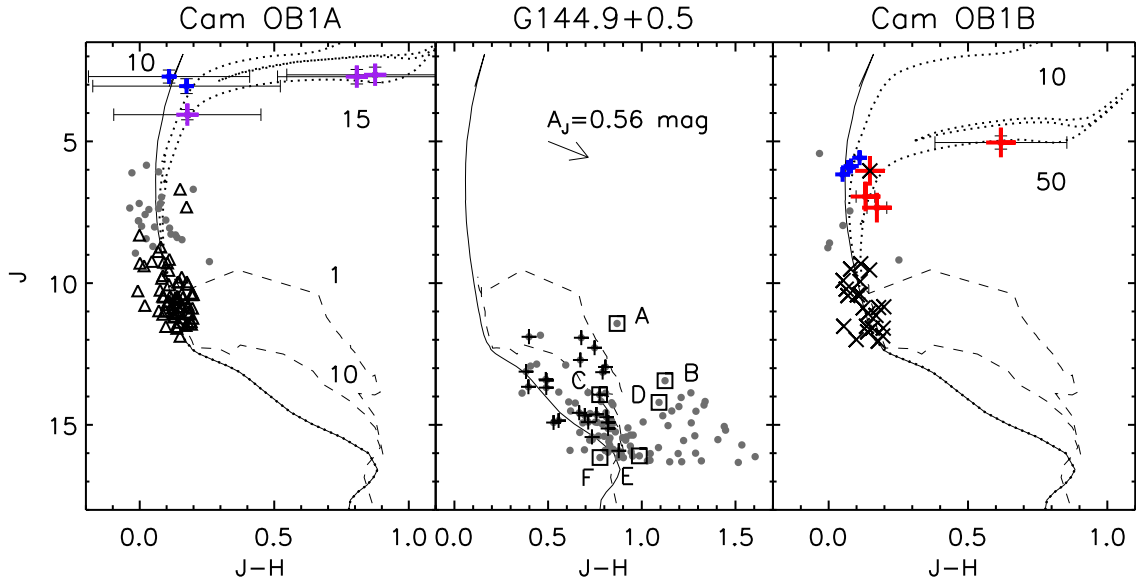


Fig. 9.— J vs. $J-H$ diagrams for Cam OB 1A (left), 1B (right), and G144 (middle). The solid line in each case delineates the ZAMS located at 1 kpc with an interstellar extinction of $A_V \sim 2.0$ mag. The dashed lines represent the pre-main-sequence isochrone for 1 and 10 Myr (Siess et al. 2000). The dotted lines represent the post-main-sequence isochrone for 10 and 15 Myr (left) and 10 and 50 Myr (right; Girardi et al. 2002). The gray dots in the left or right panels mark known 1A and 1B members, whereas those in the middle panel are stars in the cluster region. The newly found OB stars are represented by triangles (1A) and crosses (1B); purple, blue, and red pluses are supergiants (discussed in Session 3.4). In the cluster region, the pluses show the 23 PM candidates whereas the boxes represent YSO candidates (labeled).

found OB stars in 1B, like the known sample, are distributed outside the ring. The OB stars in 1B are also collectively spread toward 1A. The cloud complex in 1A and 1B has a filamentary shape (see Figure 1 in Straižys & Laugalys 2008), along which the majority of the young stars are densely populated.

It has been proposed that Cam OB1 has sustained star formation for the last 100 Myr, with a stellar age progressively younger toward the northern part of the complex (Lyder 2001). A few evolved member candidates shed crucial light on the star formation history in the region. In Figure 9, one sees a handful of candidates in 1A along the 10–15 Myr post-MS isochrones. In particular, two very bright candidates, HD 22764 (spectral type of K4 Ib) and HD 17958 (spectral type of K3 Ib), could be as old as 15 Myr. Both are well within the spatial (see Figure 10) and PM (see Figure 3) groupings like other members. Thus the age spread in 1A should be secure.

In 1B, candidates considerably older. One candidate suggests an age as old as 50 Myr. This star, HD 25056 (spectral type of G0 Ib), has a marginal PM (near the boundary circle in Figure 3) and is relatively isolated in location (see Figure 10); its membership, and hence its isochrone age, is less secure. The subgroup 1B is at least up to 10–15 Myr old. It is also possible that, from the distribution of young stars, 1B formed as the consequence of the “collect-and-collapse” mechanism (Elmegreen & Lada 1977; Deharveng et al. 2005; Zavagno et al. 2006) with which massive stars sweep ambient material via their photoionization pressure or supernova shocks, so dense clumps are collected in a shell collapse to form the next-generation stars. What we witness in G144 is the result of the most recent star birth in this cloud complex.

4. Conclusions

We used photometric, spectroscopic, and kinematic data to characterize the open cluster candidate G144 found in our OC search pipeline. The cluster is found to be a part of the Cam OB1 association. A total of 23 member candidates have been identified, some still in the pre-main sequence stage, which are distributed within an angular diameter of $\sim 7'$ at a distance of 1 kpc, this corresponds to a linear scale of ~ 2 pc across. The cluster is no more than a couple of megayears old.

Moreover, we identified a total of 91 additional OB star candidates in subgroups 1A and 1B on the basis of the PMs of 43 known OB members. Cam OB1 is associated with a molecular cloud complex and is shown to have undergone sustained star formation in subgroups 1A and 1B (and also 1C which is not studied here) for at least the last 10–

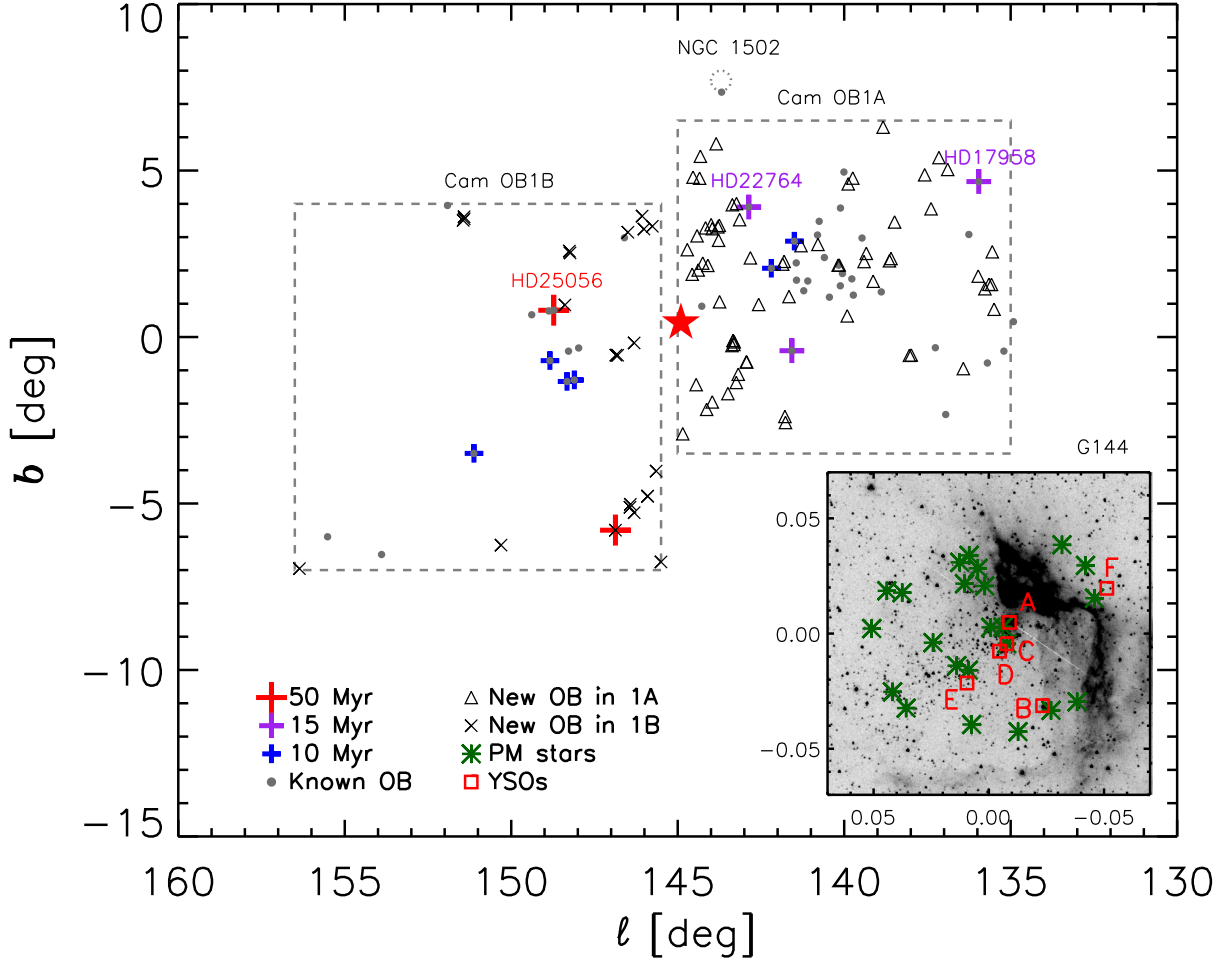


Fig. 10.— Atlas of the Cam OB1 complex and G144. Gray circles are known OB members. The dashed boxes mark the boundaries of Cam OB1A and 1B members. Black crosses and triangles mark newly found OB stars. The position of G144 is marked with a red star, whose expanded view, centered around $\ell \approx 144.9$ and $b \approx 0.4$, is shown as the inset to the bottom right. Green asterisks are PM candidates and red boxes represent YSO candidates, which are labeled individually. Members following isochrones of ages 50, 15, or 10 Myr are represented with pluses.

15 Myr. The open cluster G144 appears to highlight the latest episode of sequential star formation in the region.

We acknowledge financial support from Taiwan’s National Science Council via grants NSC101-2628-M-008-002 and NSC101-2628-M-008-001 which made this study possible. We thank the HCT staff of their assistance with acquiring the spectral data reported here during the observing run. This publication makes use of data products from the Two Micron All Sky Survey and the *Wide-field Infrared Survey Explorer*, which is a joint project of the University of Massachusetts and the Infrared Processing and Analysis Center/California Institute of Technology, funded by the National Aeronautics and Space Administration and the National Science Foundation. This work is also based on observations made with the *Spitzer Space Telescope*, which is operated by the Jet Propulsion Laboratory, California Institute of Technology under a contract with NASA. We also acknowledge use of data obtained as part of IPHAS carried out at the Isaac Newton Telescope (INT). The INT is operated on the island of La Palma by the Isaac Newton Group in the Spanish Observatorio del Roque de los Muchachos of the Instituto de Astrofísica de Canarias. All IPHAS data are processed by the Cambridge Astronomical Survey Unit, at the Institute of Astronomy in Cambridge.

REFERENCES

- Bessell, M. S., & Brett, J. M. 1988, *PASP*, 100, 1134
- Bica, E., Dutra, C. M., Soares, J. & Barbuy, B. 2003, *A&A*, 404, 223
- Cutri, R. M., Skrutskie, M. F., van Dyk, S., et al. 2003, *yCat*, 2246, 0
- Deharveng, L., Zavagno, A., & Caplan, J. 2005, *A&A*, 433, 565
- de Zeeuw, P. T., Hoogerwerf, R., de Bruijne, J. H. J., Brown, A. G. A., & Blaauw, A. 1999, *AJ*, 117, 354
- Dias, W. S., Alessi, B. S., Moitinho, A., & Lépine, J. R. D. 2002, *A&A*, 389, 871
- Drew, J. E., Greimel, R., Irwin, M. J., et al. 2005, *MNRAS*, 362, 753
- Dutra, C. M., & Bica, E. 2001, *A&A*, 376, 434
- Dutra, C. M., Bica, E., Soares, J., & Burbuy, B. 2003, *A&A*, 400, 533

- Elmegreen, B. G., & Lada, C. J. 1977, *ApJ*, 214, 725
- Froebrich, D., Scholz, A., & Raftery, C. L. 2007, *MNRAS*, 374, 399
- Girardi, L., Bertelli, G., Bressan, A., et al. 2002, *A&A*, 391, 195
- Glushkova, E. V., Koposov, S. E., Zolotukhin, I. Y., et al. 2010, *AstL*, 36, 75
- Haug, U. 1970, *A&AS*, 1, 35
- Humphreys, R. M. 1978, *ApJS*, 38, 309
- Koenig, X. P., Leisawitz, D. T., Benford, D. J., et al. 2012, *ApJ*, 744, 130
- Koposov, S., Belokurov, V., Evans, N. W., et al. 2008, *ApJ*, 686, 279
- Kronberger, M., Teutsch, P., Alessi, B., et al. 2006, *A&A*, 447, 921
- Lin, C. C., Chen, W. P., Panwar, N. 2012, in *AIP Conf. Proc.* 1543, First International Conference on Chemical Evolution of Star Forming Region and Origin of Life: *Astrochem2012*, ed. S. K. Chakrabarti, K. Acharyya, & A. Das (Melville, NY: AIP), 120
- Lyder, D. A. 2001, *AJ*, 122, 2634
- Meyer, M. R., Calvet, N., & Hillenbrand, L. A. 1997, *AJ*, 114, 288
- Monet, D. G., Levine, S. E., Canzian, B., et al. 2003, *AJ*, 125, 984
- Morgan, W. W., Whitford, A. E., & Code, A. D. 1953, *ApJ*, 118, 318
- Pandey, A. K., Upadhyay, K., Nakada, Y., & Ogura, K. 2003, *A&A*, 397, 191
- Paunzen, E., Netopil, M., Iliev, I. K., et al. 2005, *A&A*, 443, 157
- Piskunov, A. E., Kharchenko, N. V., Röser, S., Schilbach, E. & Scholz, R.-D. 2006, *A&A*, 445, 545
- Rieke, G. H., & Lebofsky, M. J. 1985, *ApJ*, 288, 618
- Röser, S., Demleitner, M., & Schilbach, E. 2010, *AJ*, 139, 2440
- Schmeja, S. 2011, *AN*, 332, 172
- Siess, L., Dufour, E., & Forestini, M. 2000, *A&A*, 358, 593

- Straižys, V., & Laugalys, V. 2007a, *BaltA*, 16, 167
- Straižys, V., & Laugalys, V. 2007b, *BaltA*, 16, 327
- Straižys, V., & Laugalys, V. 2008, in *Handbook of Star Forming Regions, Volume I. The Northern Sky*, ed. B. Reipurth, (San Francisco, CA: ASP), 294
- Tapia, M., Costero, R., Echevarria, J., & Roth, M. 1991, *MNRAS*, 253, 649
- Weitenbeck, A. J. 1997, *AJ*, 114, 222
- Wright, E. L., Eisenhardt, P. R. M., Mainzer, A. K., et al. 2010, *AJ*, 140, 1868
- Zavagno, A., Deharveng, L., Comerón, F., et al. 2006, *A&A*, 446, 171